Response of the Quasi-Biennial Oscillation to historical volcanic eruptions

K. DallaSanta[1,2], C. Orbe[1], D. Rind[1], L. Nazarenko[1,3], J. Jonas[1,3]

[1]NASA Goddard Institute for Space Studies, New York, New York, USA
[2]Universities Space Research Association, Columbia, Maryland, USA
[3]Center for Climate Systems Research, Columbia University, New York, New York, USA

Key Points:

- Historical simulations of Krakatoa and Pinatubo are studied using the high-top NASA GISS Model E2.2
- Eruptions bias the QBO towards a westerly state, and the period response depends on initial phase
- The signature of eruptions on QBO amplitude is unclear from these simulations alone

Corresponding author: Kevin DallaSanta, `kevin.dallasanta@nasa.gov`

Abstract

The impact of volcanic eruptions on surface climate is well-appreciated, but their *in situ* impact on the Quasi-Biennial Oscillation (QBO) has received comparatively little attention. This study examines the QBO responses to Krakatoa and Pinatubo using five configurations of the NASA Goddard Institute for Space Studies (GISS) Model E2.2 and MERRA-2 reanalysis. A dynamically consistent response is found in terms of static stability, zonal wind, and upwelling. Eruptions are found to bias the QBO towards a westerly state, such that the QBO period response depends upon the phase at the time of eruption. The QBO does not have a clear amplitude response to an eruption, based on these simulations. The underlying mechanisms appear not to be influenced to first-order by interactive composition, sea surface temperatures, or long-term trends in CO_2 and ozone-depleting substances.

Plain Language Summary

In the tropical stratosphere, the winds alternate between easterly and westerly, taking about 28 months to return to their original state. This "Quasi-Biennial Oscillation" (QBO) is ordinarily quite stable, but it can be disturbed by large forcings such as geoengineering and volcanic eruptions. In this study, we consider two volcanic eruptions in the historical record—Krakatoa (1883) and Pinatubo (1991)—and their subsequent effect on the QBO. We simulate them using a climate model, and find that the QBO prefers a westerly state after eruptions. This is important because the QBO state affects surface climate and weather prediction. Our results are largely consistent with observations of Pinatubo, and they can be tested in other climate models.

1 Introduction

It is well-appreciated that large tropical eruptions impact the atmosphere. Injected sulfate aerosols cool the surface and warm the lower stratosphere through absorption of shortwave radiation (Robock, 2000). The impacts of this forcing on the troposphere and extratropical stratosphere have received a great deal of attention, including: an acceleration of the polar vortex (e.g., Graf et al., 1993), changes to planetary waves (e.g., Stenchikov et al., 2002), a reduction in global precipitation (e.g., Iles et al., 2013), and altered surface temperatures (e.g., Robock & Mao, 1995) including winter warming.

However, the *in situ* impact of volcanic aerosols on the Quasi-Biennial Oscillation (QBO) has received much less attention. Some studies have considered geoengineering and supereruptions, which impact the tropical stratosphere on longer timescales than more moderately-sized eruptions. The general finding is that aerosol heating leads to anomalous westerlies, consistent with thermal wind balance (Randel et al., 1999), despite the large Rossby number at low latitudes. Aquila et al. (2014) simulated geoengineering as a time-invariant aerosol forcing and found that sufficiently large SO_2 injections could lengthen or shutdown the QBO in a westerly state, moderated by changes in upwelling. Niemeier and Schmidt (2017) explored a wider variety of forcing scenarios and obtained similar results, noting a dependence on initial QBO phase for transport. Richter et al. (2017) also obtained similar results, finding that interactive chemistry apparently buttressed the QBO against an aerosol-driven shutdown. Lastly, Brenna et al. (2021) simulated the supereruption of Los Chocoyos (75,000 years before present) and found a more complex response, with a long easterly pause followed by a westerly pause.

Hence, the transient impact on the QBO from more moderately sized eruptions is not clear *a priori*, and it appears that little work has been done on the subject. This is the focus of our study. Capturing the correct QBO response after an eruption is important for seasonal prediction (e.g., Garfinkel et al., 2018), QBO teleconnections (e.g., Marshall & Scaife, 2009), and trace gases (e.g., Tweedy et al., 2017). It is also desirable from a perspective of model verification that models credibly capture the forced response to eruptions. In particular, our model captures a wide range of feedbacks: interactive sourcing of gravity wave drag, a coupled ocean, and interactive chemistry. Of the four studies mentioned above, three employed fixed non-orographic gravity wave drag, and two had specified sea surface temperatures, which may limit dynamical pathways for the QBO to respond to volcanic activity.

2 Experimental setup

In this study, we focus on eruptions in historical integrations from 1850 to 2015. The integrations are performed with the 102-layer high-top NASA Goddard Institute for Space Studies (GISS) Model E2.2 (Rind et al., 2020; Orbe et al., 2020), a contributor to the Sixth Coupled Model Intercomparison Project (CMIP6). The model's QBO is tethered to convection through an interactive gravity wave drag scheme (Rind et al., 1988, 2014). Historical forcings are as described in Miller et al. (2021); however, the model used in that study had only 40 vertical levels and did not resolve a QBO. Explosive volcanic forcing is purely prescribed, using CMIP6 monthly aerosol extinction coefficients (Arfeuille et al., 2014; Thomason et al., 2018), linearly interpolated in time. In general, aerosol forcing is highly uncertain for both observations (Arfeuille et al., 2013) and models (Clyne et al., 2021), so we focus on dynamical aspects which may be consistent with other simulations.

We implement the model in a variety of configurations to test robustness and mechanisms. Each configuration is integrated from 1850 to 2015 in ensembles of 4 or 5 members. The configurations vary according to:

1. SP/AP physics: Standard Physics (SP) and Altered Physics (AP). As described in Rind et al. (2020); Orbe et al. (2020), the configurations differ by a number of technical changes linking model physics with vertical resolution. For our purposes, comparison between SP and AP suggests which of our results may not be robust among other CMIP6 models.
2. OCN/AMIP sea surface temperatures: interactive ocean (OCN) with 40 vertical layers or atmosphere-only (AMIP) with specified observations.
3. OMA/NINT composition: interactive chemistry (OMA; Bauer et al., 2020) or non-interactive chemistry (NINT) with monthly mean composition forcing prescribed from the zonally varying ensemble average of the corresponding OMA AMIP runs.

To investigate the QBO response to volcanoes, we focus on Krakatoa (1883) and Pinatubo (1991). These eruptions are largest in terms of tropically averaged aerosol optical depth (AOD). For Pinatubo, we compare simulations with MERRA-2 reanalysis (Gelaro et al., 2017), using dynamic diagnostics computed by Martineau et al. (2018).

To analyze changes to the QBO, we use the definitions of phase, period, and amplitude presented in DallaSanta et al. (2021). This approach considers the first two principal components of zonally averaged equatorial zonal wind between 10 and 100 hPa, which capture approximately 95% of variance. QBO amplitude is the magnitude of the two principal components, QBO phase is their orientation in phase space, and QBO period is the time elapsed for its phase to progress 360°.

3 Response of the tropical stratosphere to eruptions

In this section, we trace the stratospheric impact of eruptions from aerosol heating to the zonal wind field and hence the QBO. We begin by examining forced AOD, the subsequent heating rate, and the final temperature response. These fields are presented in Figure 1 for one example integration (others are similar) and for reanalysis.

The timescale of the equatorial aerosols (row 1) is one to two years, and is somewhat weaker and longer for Pinatubo than for Krakatoa. The amplitude difference is primarily due to their respective latitudes, as the tropical stratosphere experiences smaller aerosol loading under Pinatubo than Krakatoa. Both are subject to uncertainties: pre-1979 values in the CMIP6 dataset are parameterized (Arfeuille et al., 2014), and post-Pinatubo the AOD lifetime is too long in both the model and MERRA-2 (Buchard et al., 2017). (Since MERRA-2 only provides AOD from all aerosols, we have deseasonalized it using the volcanically quiescent years 1984–1991, such that the remainder is a reasonable approximation to volcanic AOD alone.)

Despite ambiguity in historical AOD, its radiative impact is more clear. Specifically, the presence of the aerosols induces anomalous heating in the mid-stratosphere (row 2) from both shortwave and longwave contributions (Supplementary Figure S1). The strongest heating rates correspond to the onset of the aerosol forcing and its decay, and are confined to the aerosol location (above about 40 hPa). For Pinatubo, the aerosol appears to have a more seasonal pulse, consistent with Pinatubo's off-equatorial location.

The net effect is a substantial temperature perturbation superimposed upon the existing temperature QBO (row 3). For the model example shown, a descending cold branch is interrupted by Krakatoa, and a descending warm branch is strengthened by Pinatubo. In reanalysis, a descending cold branch is interrupted by Pinatubo. Thus, the temperature QBO can be overwhelmed by aerosol heating, as was found for the long-term in the geoengineering and supervolcano studies previously discussed. The temperature anomalies persist beyond the aerosol timescale and propagate downwards below the initial heating level. This indicates that the anomalies behave as QBO secondary circulations (Randel et al., 1999; DallaSanta et al., 2019) superimposed upon the background state. We will diagnose these circulations in terms of stability, upwelling, and zonal wind. Furthermore, as these anomalies propagate down, critical layer absorption provides a pathway for them to modify the QBO at higher levels (DallaSanta et al., 2021), even after the aerosols have decayed. Hence, the background state of the QBO is critical for the subsequent QBO response. In the remainder of the paper, we quantify this response more precisely.

To do so, we first present all model members alongside reanalysis. Given the timescales of Figure 1 and the importance of the seasonal cycle, we time-average over the one-year interval following each eruption. In the extratropics, temperature and zonal wind are quantitatively related by thermal wind balance. This relationship becomes more qualitative at lower latitudes, due to the vanishing of the Coriolis parameter. Hence, temperature and zonal wind evolve in tandem with changes to upwelling and wave breaking. We convert temperature to static stability $S_p = -T\,\partial \ln\theta/\partial p$ to facilitate comparison. The resulting anomalies are shown in Figure 2. We interpret the key points as follows:

1. There is a consistent relationship between the static stability, zonal wind, and upwelling responses. This can be seen as a correlation among the vertical profiles of each member, color-coded by their initial phase.
2. Variation in the sign, magnitude, and height of these responses is closely related to differences in initial QBO phase. For instance, in a westerly phase (light blue), an increase in static stability above 20 hPa inhibits upwelling above this level, and a decrease in static stability below 20 hPa enhances upwelling below.
3. Krakatoa and Pinatubo are very comparable in their effects on static stability, zonal wind, and upwelling. This occurs despite the difference in aerosol loading (Figure 1) and the difference in background conditions, suggesting that long-term climatology is not a primary factor for the results.
4. The NINT runs have comparable dynamical responses to OMA, despite having prescribed composition that does not correspond to their initial QBO phase. This implies that variations in composition are also less important for obtaining the correct dynamical response.

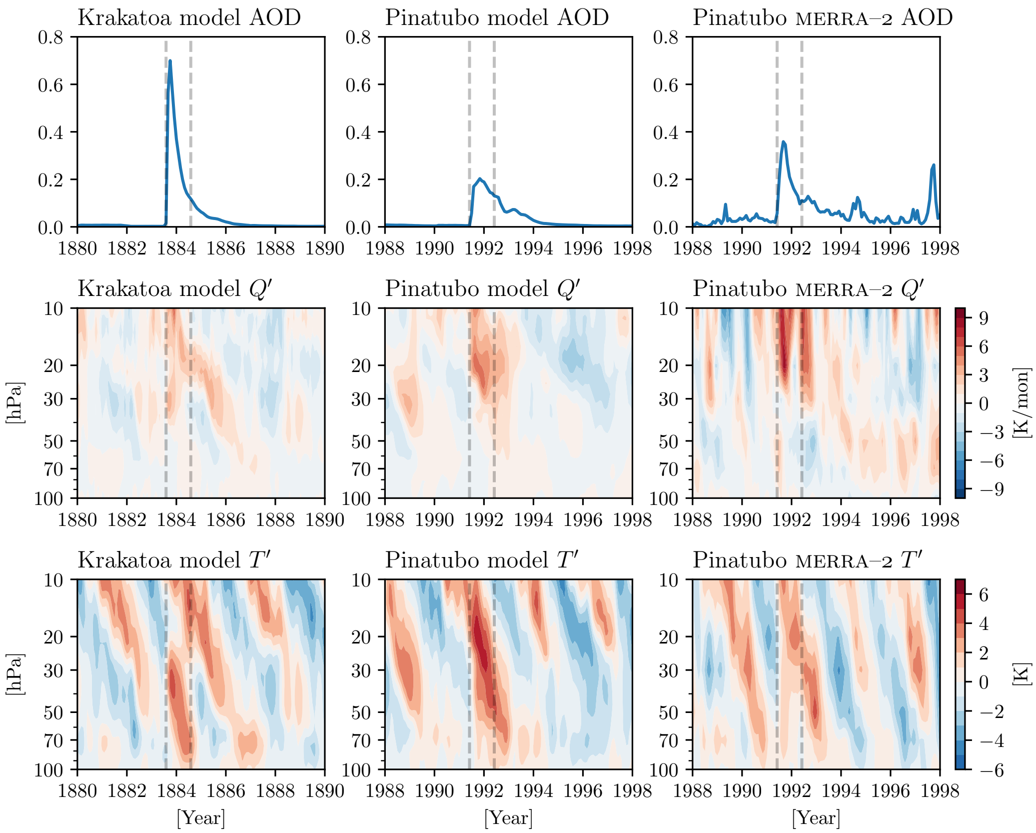

Figure 1. Equatorial AOD, aerosol heating (Q'), and temperature anomalies (T') for an example integration (columns 1 and 2) and for MERRA-2 reanalysis (column 3). Anomalies are defined as departures from the climatological average over the decade preceding the eruption. Since diagnostics solely of volcanic aerosol heating are not available, proxies are taken as the solar heating rate (model) and the longwave clear sky heating rate (reanalysis), with the seasonal and quasi-biennial cycles subtracted. The dashed lines indicate the one-year interval following the eruption, used for subsequent analysis. Values are gently smoothed for plotting, using a 3-month filter.

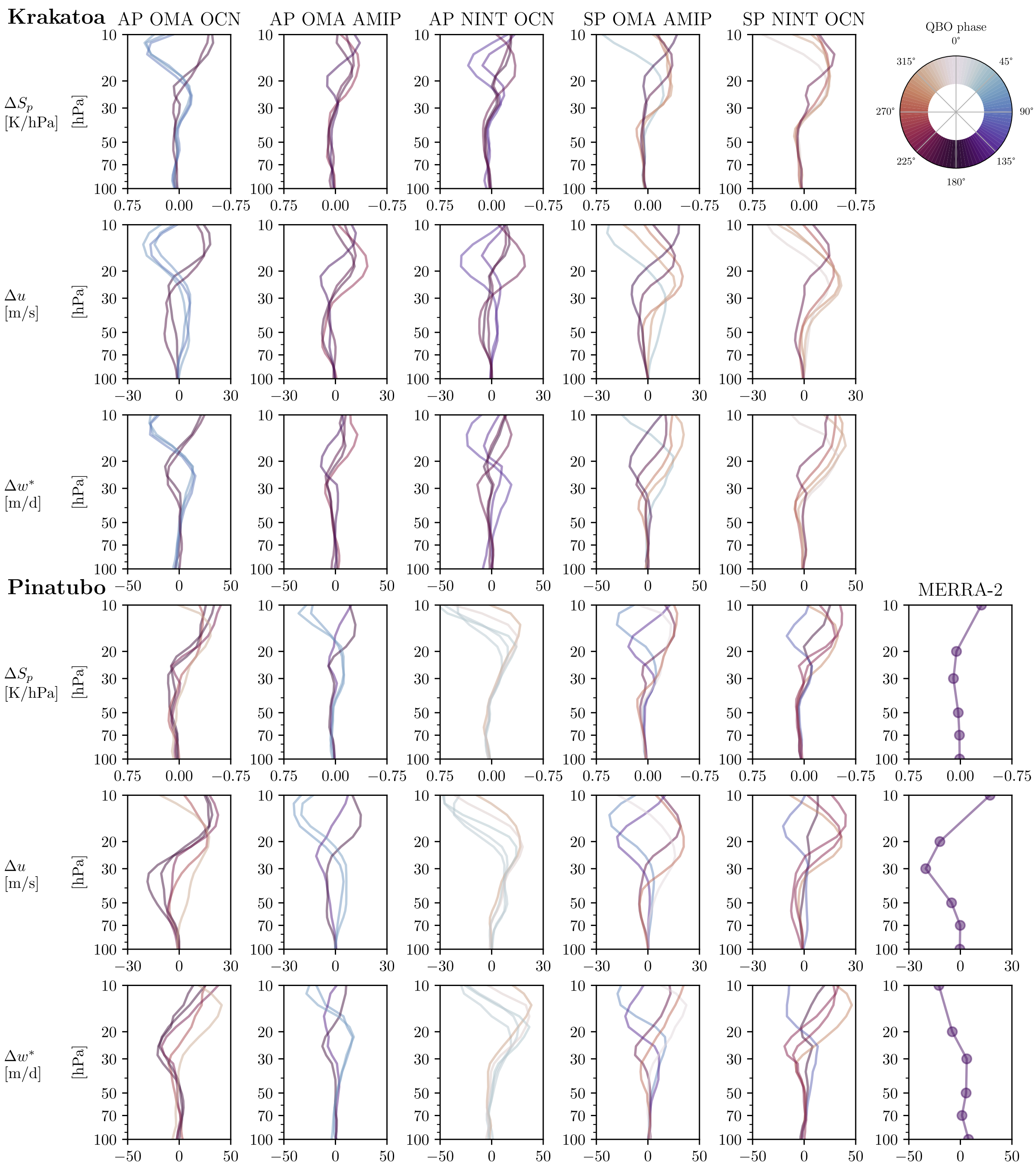

Figure 2. Responses of tropical static stability (S_p, shown with reversed abscissa), zonal wind (u), and residual vertical velocity (w^*), expressed as anomalies Δ from the decadal climatology, averaged over the one-year interval after Krakatoa (rows 1–3) and Pinatubo (rows 2–4). Each line denotes an individual ensemble member. Static stability and zonal wind are equatorial, for consistency with QBO analysis; vertical velocity is tropically averaged from $[-10, 10]$ degrees latitude, due to its high spatial variability. The colorwheel indicates the QBO phase at the time of eruption, to show which members have similar/contrasting initial phases. Dots indicate MERRA-2 levels provided by (Martineau et al., 2018).

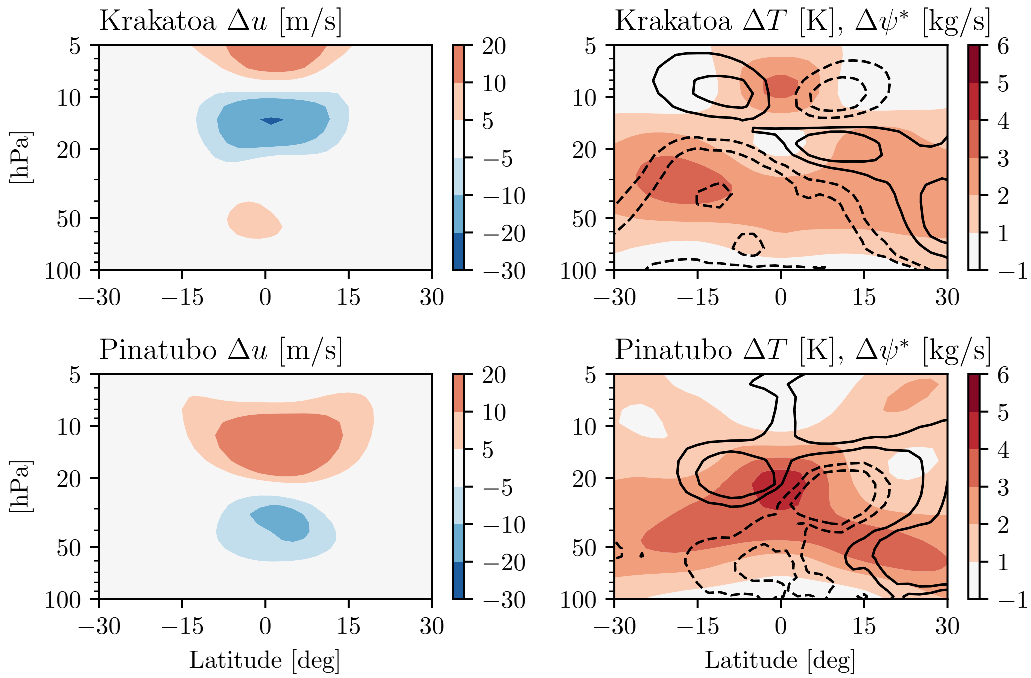

Figure 3. Responses of tropical zonal wind (column 1), temperature (column 2, colors), and residual circulation (column 2, arbitrary contours) for the example in Figure 1. As before, these are expressed as anomalies Δ from the decadal climatology, averaged over the one-year interval after Krakatoa (row 1) and Pinatubo (row 2).

5. Similarly, ocean variability does not appear to be critical, given the modest differences (Supplementary Table S1). However, variability in sea surface temperatures can impact convection, which we will argue matters for the QBO response only if it is sufficiently weak.
6. MERRA-2 has a comparable dynamical response to the model, in terms of its amplitude, vertical structure, and dependence on initial phase. This is despite the fact that the model does not capture the observed ozone response in its entirety, at least above 30 hPa (Supplementary Figure S2), due to underestimated chlorine activation in the post-CFC background state (Tie & Brasseur, 1995; Klobas et al., 2017; Hegglin & Tegtmeier, 2017). Thus, the ozone response does not appear to be fundamental to capturing the overall dynamical response.
7. The AP and SP configurations yield consistent results, suggesting that these dynamical responses are not highly sensitive to model physics. However, such a sensitivity becomes more apparent in QBO phase space, as we will demonstrate.

Physically, the response is interpretable as a secondary circulation (Randel et al., 1999; DallaSanta et al., 2019), as seen in Figure 3. Although the mean circulation is predominately mechanically driven, the anomaly is largely thermally forced (c.f. Garcia, 1987), and the heating contribution to $\Delta\psi^*$ exceeds the mechanical contribution (not shown). Thus, a localized decrease in stability is associated with enhanced upwelling and associated westerly torque, and vice versa. As this example member shows, the altitude of this circulation again depends on initial QBO phase, which we now examine more closely.

3.1 Response of QBO period to eruptions

In this section, we explore the quantitative responses of the QBO period and amplitude to eruptions. Overall, we find that aerosol injections bias the QBO towards a westerly phase (see Figure 4a for reference). This is consistent with the aforementioned geoengineering and supervolcano studies. For our simulations, where aerosols decay on a timescale of one to two years, it may be expected that an eruption during a westerly phase prolongs the QBO, and an eruption during an easterly phase hastens the QBO. This is qualitatively suggested by Figure 1, and quantitatively confirmed by Figure 4bc, which shows the QBO period for each member immediately following the eruption. As expected, models in a westerly phase at the time of eruption (i.e., left of the dotted line) have substantially longer periods than climatology (horizontal lines), up to a factor of 2. In contrast, models in an easterly phase at the time of eruption (i.e., right of the dotted line) have faster periods than climatology. We now discuss these features in greater detail.

As a function of initial phase, the QBO response is fairly smooth with a discontinuity near the westerly onset ($\phi \approx 140°$) at 10 hPa. As the initial phase approaches this critical value, heating by volcanic aerosols prolongs the westerly phase. To the right of the discontinuity, the aerosol heating interferes with the easterly phase of the QBO, hastening the downward migration of the westerly branch. This acceleration is more clear for Krakatoa than Pinatubo, likely because Krakatoa has a larger aerosol injection in the QBO region (Figure 1). For Pinatubo, MERRA-2 lies to the right of the discontinuity, with a period slightly shorter than its average value, although the initial response was a westerly lengthening (Labitzke, 1994).

Notably, the SP OMA AMIP ensemble (in red) appears to be an exception to the QBO period results. Its members near the critical phase have little departure from climatology. We attribute this limitation to the ensemble's weak momentum flux due to convection. Specifically, the zonal wind tendency due to convective gravity wave drag is in-phase with the total tendency, and short-term variations in phase speed are positively correlated with momentum flux due to convection (DallaSanta et al., 2021). Ignoring all other contributions to the wind tendencies, one can thus derive a lower bound on the QBO period resulting solely from momentum deposition associated with parameterized convective gravity wave drag, as detailed in the Appendix. Figure 4de shows the QBO periods as a function of post-volcanic momentum flux due to convection, comparing them with these respective lower bounds inferred from climatology. Essentially, the weak momentum flux in SP OMA AMIP limits the rate at which the QBO can descend, such that the post-eruption response is close to the theoretical maximum phase progression (i.e., the theoretical minimum period). Even if these members begin in the optimal phase $\phi > 140°$, the relatively weak convection inhibits their period response, unlike the other ensembles. Our estimate involves a number of assumptions and quantitative uncertainties, but it is nevertheless qualitatively helpful for understanding why some members may be outliers.

Thus, we draw the following interpretation. First, the QBO period response in the model is set by the initial QBO phase, with a bias towards a westerly state and away from an easterly state, related to the onset of upper-level westerlies. Second, if the model is initially in an easterly state—optimal for enhancing the subsequent phase speed—then insufficient convection will limit the period response obtained. The intra-ensemble spread in convective flux is less than the inter-ensemble spread, pointing to differences in model configuration as key rather than sample uncertainty. The OCN ensembles have larger intra-ensemble spread than AMIP, indicating that both the sea surface and the free atmosphere increase variance.

To summarize, eruptions bias the QBO phase towards lower stratospheric westerlies, such that the QBO progresses relatively slowly when initialized in a westerly phase, and relatively quickly when initialized in an easterly phase. In the latter case, the avail-

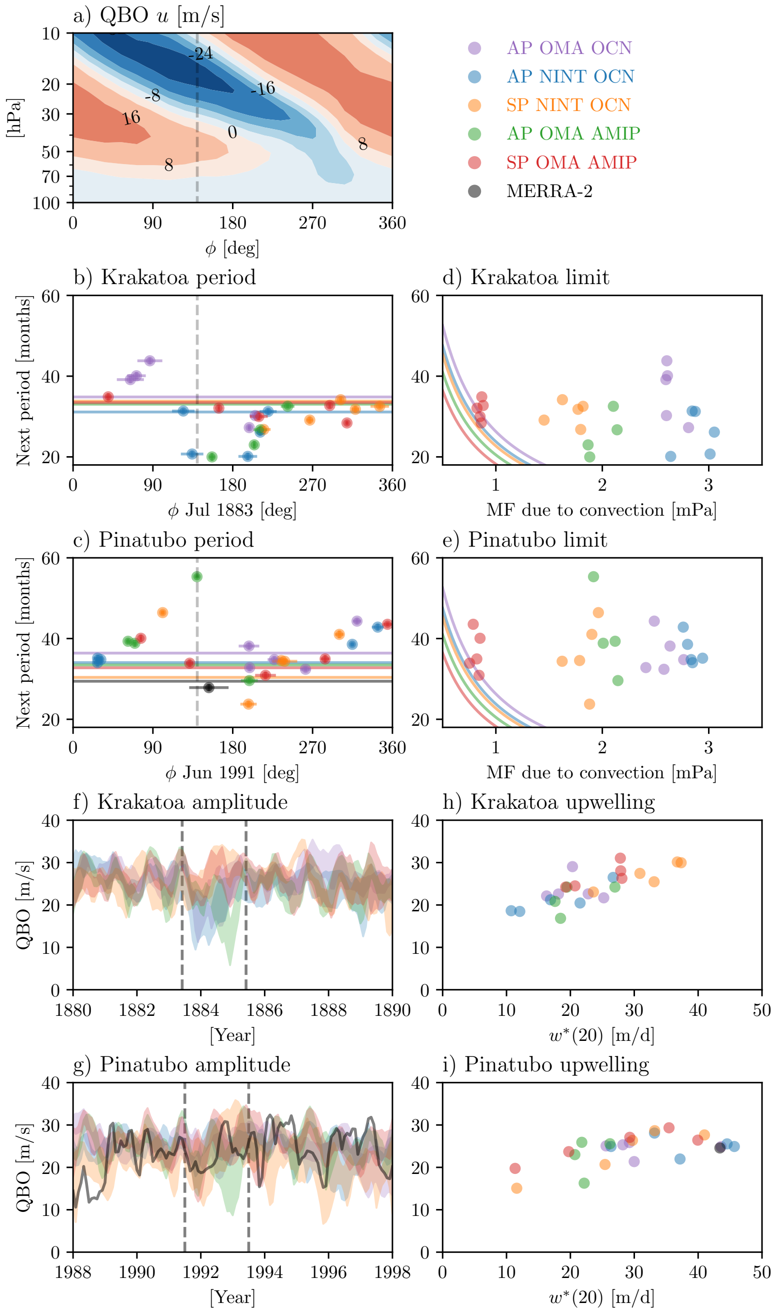

Figure 4. (a) Composited equatorial zonal wind as a function of QBO phase ϕ, shown for reference and labeled in m/s. The dotted line indicates the westerly onset. (b,c) Responses of the QBO period to eruptions, quantified as the length of the period immediately following each eruption. Colors denote ensembles as labeled. Horizontal lines indicate the climatological period for each ensemble. Crosses indicate uncertainty stemming from the sampling frequency. (d,e) Responses of the QBO period to eruptions, but as a function of momentum flux due to convection averaged over the one-year interval following the eruption. Momentum flux is tropically averaged from $[-5, 5]$ degrees latitude, which maximizes correspondence with phase speed (DallaSanta et al., 2021). The colored curves indicate the estimated lower bound for each ensemble, as discussed in text. (f,g) QBO amplitude around eruptions, shown as the $\pm 2\sigma$ range for each ensemble. Dashed lines indicate the 2-year period following the eruption. (h,i) QBO amplitude and 20 hPa residual vertical velocity w^*, averaged over the 2-year period after each eruption. Vertical velocity is tropically averaged from $[-10, 10]$ degrees latitude.

ability of momentum flux due to convection can limit the resulting QBO progression in our model.

3.2 Response of QBO amplitude to eruptions

Lastly, we consider the impact of volcanic eruptions on QBO amplitude, plotted in Figure 4fg. The results suggest that the AP configurations have some probability of a weakened amplitude post-eruption, but the SP configurations and MERRA-2 reanalysis do not. The timescale of these amplitude responses appears to be within the first two years of the eruption, and the response is not uniform among members, indicating that internal variability is at play.

To quantify individual members, we plot in Figure 4hi the amplitude as a function of vertical velocity. The amplitude evidently varies by a factor of 2, and is strongly correlated with vertical velocity at 20 hPa. MERRA-2 reanalysis lies within the model spread, supporting the model results. Therefore, simple correlation suggests that the QBO amplitude decrease is associated with reduced upwelling in that region.

Intriguingly, the amplitude response is positively rather than negatively correlated with upwelling. Could the short-term QBO response to perturbations involve a positive correlation, rather than the negative correlation generally seen for long-term trends (e.g., Kawatani & Hamilton, 2013; Richter et al., 2020; DallaSanta et al., 2021)? This is difficult to assess from these simulations alone, as any relationship could be direct (through advection) or indirect (e.g., involving changes to planetary wave activity). In particular, we find that the correlation between QBO amplitude and upwelling depends upon vertical level. However, 20 hPa was a key altitude for many members in Figure 2, suggesting that any QBO amplitude response may be associated with the secondary circulation. This imparts a complexity to the amplitude–upwelling relationship that has become more recently appreciated, even in the context of longer-term CO_2-induced trends (Richter et al., 2020). Given this complexity, we refrain from drawing a mechanistic interpretation of the amplitude weakening, without additional investigation.

Further analysis of individual members does not find a relation between initial phase and the QBO amplitude response, in the same way a relationship was found for the QBO period. Hence we cannot confidently conclude that eruptions weaken QBO amplitude, as any response appears to be sensitive to model physics (SP versus AP) and the details of a given eruption (Krakatoa versus Pinatubo). This null-hypothesis result underscores the importance of using multiple configurations: had we only integrated AP, we would have concluded that volcanic eruptions do lower QBO amplitude.

4 Conclusions

We have studied the impact of Krakatoa and Pinatubo on the QBO using the NASA GISS Model E2.2. Our main conclusions are:

1. Krakatoa and Pinatubo have a similar signature on static stability, zonal wind, and upwelling. The responses of these fields are dynamically consistent as residual circulation anomalies, and their sign and height are strongly modulated by the initial QBO phase.
2. Volcanic eruptions bias the QBO towards lower-stratospheric westerlies via aerosol-induced heating, such that the QBO period response to eruptions also depends on initial QBO phase.
3. When the eruption occurs after the onset of upper-level westerlies, the model's period response is further modulated by the availability of momentum flux due to convection. This is related to the convective sourcing of gravity wave drag.

4. The amplitude response is overall unclear. There is no decrease for reanalysis and the SP configurations, but there is some decrease in the AP configurations.

With respect to the geoengineering and supereruption simulations discussed in the introduction, our results are broadly in dynamical agreement. Aerosol forcing nudges the models toward a westerly phase, mediated primarily by changes in upwelling. We hypothesize that under longer-term sulfate loading (from geoengineering or supereruptions) our model QBO would similarly be prolonged and eventually freeze in a westerly phase. However, Brenna et al. (2021) found an initial easterly response to supereruptions. Our more moderately sized eruptions do not appear to induce an initial easterly response. We intend to investigate these aspects along with the QBO amplitude in a future study, using a range of more targeted simulations. The impact of interactive aerosols also merits further attention, as the magnitude of the response (and other quantitative details) may depend on the background state and the evolution of the aerosols.

The amplitude decreases for some of the AP ensemble members suggests that the QBO may be more unstable after an eruption. As previous work has found the QBO to shutdown in response to sufficiently strong forcing, we plan to test a wider range of forcing amplitudes to explore possible collapse and recovery.

We conjectured that the period response to eruptions may have a lower bound if convection is sufficiently weak. The true magnitude of tropical gravity wave momentum flux is on the same order as the model configurations, but is difficult to estimate precisely (Geller et al., 2013), so we do not know if it lies near this hypothetical lower bound. A physical link between convection and gravity wave drag is recognized (e.g., Alexander et al., 2010), so more precise observations or future high-resolution simulations would provide insight regarding the relevance of our result.

The clear signal in the QBO period response, underscored by its dynamical rationale, suggests that it should be straightforward to test our findings in other QBO-resolving models, even with one or few members. We hypothesize that models with fixed gravity wave sources might obtain a similar period result, as long as the prescribed momentum flux exceeds the estimated lower bound. Further investigation may be fruitful using historical output available from other CMIP6 models.

Appendix A Period limit set by convective flux

We estimate a lower bound on the model's QBO period. Considering the composited momentum budget (DallaSanta et al., 2021), the downward propagation of the QBO is predominantly driven by tropical momentum flux due to convection, which is in-phase with the total tendency. Suppose that all of this momentum flux, and only this momentum flux, is used to drive the QBO. Let u_t be the composited zonal wind tendency as a function of phase ϕ and level p, and let $\phi_t = u_t/u_\phi$ be the phase speed. Then:

$$\text{momentum flux} = \int_0^{p_s} |u_t|/g \; \mathrm{d}p = \phi_t \int_0^{p_s} |u_\phi|/g \; \mathrm{d}p \equiv \phi_t I \tag{A1}$$

Here $I(\phi)$ is the inertia of the QBO, requiring momentum deposition to drive its characteristic downward propagation. We find *a posteriori* that I is reasonably uniform as a function of phase, so both sides can be averaged in ϕ. This yields an estimated maximum phase velocity associated with momentum flux due to convection. The equivalent period is obtained by inverting this phase velocity. Composites are constructed across the ensemble average of each configuration; the resulting lower bound on the period is shown for each ensemble in Figure 4de.

Acknowledgments

We thank the editor and two anonymous reviewers for their constructive feedback. KD acknowledges support from the NASA Postdoctoral Program at the Goddard Institute for Space Studies. Resources supporting this work were provided by the NASA High-End Computing (HEC) Program through the NASA Center for Climate Simulation (NCCS) at Goddard Space Flight Center.

Data availability: All integrations are uploaded at `https://zenodo.org/record/512925`. ModelE source code is maintained at `https://www.giss.nasa.gov/tools/modelE/`. MERRA-2 reanalysis data are maintained at `https://disc.gsfc.nasa.gov`.

References

Alexander, M. J., Geller, M., McLandress, C., Polavarapu, S., Preusse, P., Sassi, F., … Watanabe, S. (2010). Recent developments in gravity-wave effects in climate models and the global distribution of gravity-wave momentum flux from observations and models. *Quarterly Journal of the Royal Meteorological Society*, *136*(650), 1103–1124.

Aquila, V., Garfinkel, C. I., Newman, P. A., Oman, L. D., & Waugh, D. W. (2014). Modifications of the quasi-biennial oscillation by a geoengineering perturbation of the stratospheric aerosol layer. *Geophys. Res. Lett.*, *41*(5), 1738–1744.

Arfeuille, F., Luo, B. P., Heckendorn, P., Weisenstein, D., Sheng, J. X., Rozanov, E., … Peter, T. (2013). Modeling the stratospheric warming following the Mt. Pinatubo eruption: Uncertainties in aerosol extinctions. *Atmospheric Chemistry and Physics*, *13*(22), 11221–11234.

Arfeuille, F., Weisenstein, D., MacK, H., Rozanov, E., Peter, T., & Brönnimann, S. (2014). Volcanic forcing for climate modeling: A new microphysics-based data set covering years 1600–present. *Climate of the Past*, *10*(1), 359–375.

Bauer, S. E., Tsigaridis, K., Faluvegi, G., Kelley, M., Lo, K. K., Miller, R. L., … Wu, J. (2020). Historical (1850–2014) Aerosol Evolution and Role on Climate Forcing Using the GISS ModelE2.1 Contribution to CMIP6. *Journal of Advances in Modeling Earth Systems*, *12*(8), 0–3.

Brenna, H., Kutterolf, S., Mills, M. J., Niemeier, U., Timmreck, C., & Krüger, K. (2021). Decadal Disruption of the QBO by Tropical Volcanic Supereruptions. *Geophysical Research Letters*, *48*(5).

Buchard, V., Randles, C. A., da Silva, A. M., Darmenov, A., Colarco, P. R., Govindaraju, R., … Yu, H. (2017). The MERRA-2 aerosol reanalysis, 1980 onward. Part II: Evaluation and case studies. *Journal of Climate*, *30*(17), 6851–6872.

Clyne, M., Lamarque, J. F., Mills, M. J., Khodri, M., Ball, W., Bekki, S., … Toon, O. B. (2021). Model physics and chemistry causing intermodel disagreement within the VolMIP-Tambora Interactive Stratospheric Aerosol ensemble. *Atmospheric Chemistry and Physics*, *21*(5), 3317–3343.

DallaSanta, K., Gerber, E. P., & Toohey, M. (2019). The circulation response to volcanic eruptions: The key roles of stratospheric warming and eddy interactions. *Journal of Climate*, *32*(4), 1101–1120.

DallaSanta, K., Orbe, C., Rind, D., Nazarenko, L., & Jonas, J. (2021). Dynamical and Trace Gas Responses of the Quasi-Biennial Oscillation to Increased CO2. *Journal of Geophysical Research: Atmospheres*, *126*(6), 1–28.

Garcia, R. R. (1987). On the Mean Meridional Circulation of the Middle Atmosphere. *J. Atmos. Sci.*, *44*(24), 3599–3609.

Garfinkel, C. I., Schwartz, C., Domeisen, D. I., Son, S. W., Butler, A. H., & White, I. P. (2018). Extratropical Atmospheric Predictability From the Quasi-Biennial Oscillation in Subseasonal Forecast Models. *Journal of Geophysical Research: Atmospheres*, *123*(15), 7855–7866.

Gelaro, R., McCarty, W., Suárez, M. J., Todling, R., Molod, A., Takacs, L., …

others (2017). The modern-era retrospective analysis for research and applications, version 2 (merra-2). *Journal of climate*, *30*(14), 5419–5454.

Geller, M. A., Alexander, J. J., Love, P. T., Bacmeister, J., Ern, M., Hertzog, A., ... Zhou, T. (2013). A comparison between gravity wave momentum fluxes in observations and climate models. *Journal of Climate*, *26*(17), 6383–6405.

Graf, H.-F., Kirchner, I., Robock, A., & Schult, I. (1993). Pinatubo eruption winter climate effects: models versus observations. *Climate Dynamics*, *9*, 81–93.

Hegglin, M. I., & Tegtmeier, S. (2017). *The SPARC Data Initiative: Assessment of stratospheric trace gas and aerosol climatologies from satellite limb sounders* (Vol. 8; Tech. Rep.). ETH Zürich.

Iles, C. E., Hegerl, G. C., Schurer, A. P., & Zhang, X. (2013). The effect of volcanic eruptions on global precipitation. *Journal of Geophysical Research Atmospheres*, *118*(16), 8770–8786.

Kawatani, Y., & Hamilton, K. (2013). Weakened stratospheric quasibiennial oscillation driven by increased tropical mean upwelling. *Nature*, *497*(7450), 478–481.

Klobas, J. E., Wilmouth, D. M., Weisenstein, D. K., Anderson, J. G., & Salawitch, R. J. (2017). Ozone depletion following future volcanic eruptions. *Geophysical Research Letters*, *44*(14), 7490–7499.

Labitzke, K. (1994). Stratospheric temperature changes after the pinatubo eruption. *Journal of Atmospheric and Terrestrial Physics*, *56*(9), 1027–1034.

Marshall, A. G., & Scaife, A. A. (2009). Impact of the QBO on surface winter climate. *Journal of Geophysical Research: Atmospheres*, *114*(June), 2–7.

Martineau, P., Wright, J. S., Zhu, N., & Fujiwara, M. (2018). Zonal-mean data set of global atmospheric reanalyses on pressure levels. *Earth System Science Data*, *10*(4), 1925–1941.

Miller, R. L., Schmidt, G. A., Nazarenko, L. S., Bauer, S. E., Kelley, M., Ruedy, R., ... Yao, M. S. (2021). CMIP6 Historical Simulations (1850–2014) With GISS-E2.1. *Journal of Advances in Modeling Earth Systems*, *13*(1), 1–35.

Niemeier, U., & Schmidt, H. (2017). Changing transport processes in the stratosphere by radiative heating of sulfate aerosols. *Atmospheric Chemistry and Physics*, *17*(24), 14871–14886.

Orbe, C., Rind, D., Jonas, J., Nazarenko, L., Faluvegi, G., Murray, L. T., ... others (2020). Giss model e2. 2: A climate model optimized for the middle atmosphere—2. validation of large-scale transport and evaluation of climate response. *Journal of Geophysical Research: Atmospheres*, *125*(24), e2020JD033151.

Randel, W. J., Wu, F., Swinbank, R., Nash, J., & O'Neill, A. (1999). Global QBO circulation derived from UKMO stratospheric analyses. *Journal of the Atmospheric Sciences*, *56*(4), 457–474.

Richter, J. H., Anstey, J. A., Butchart, N., Kawatani, Y., Meehl, G. A., Osprey, S., & Simpson, I. R. (2020). Progress in Simulating the Quasi-Biennial Oscillation in CMIP Models. *Journal of Geophysical Research: Atmospheres*, *125*(8), 1–14.

Richter, J. H., Tilmes, S., Mills, M. J., Tribbia, J. J., Kravitz, B., Macmartin, D. G., ... Lamarque, J. F. (2017). Stratospheric dynamical response and ozone feedbacks in the presence of SO2 injections. *Journal of Geophysical Research: Atmospheres*, *122*(23), 12,557–12,573.

Rind, D., Jonas, J., Balachandran, N. K., Schmidt, G. A., & Lean, J. (2014). The QBO in two GISS global climate models: 1. Generation of the QBO. *Journal of Geophysical Research: Atmospheres*, *119*(14), 8798–8824.

Rind, D., Orbe, C., Jonas, J., Nazarenko, L., Zhou, T., Kelley, M., ... Schmidt, G. (2020). GISS Model E2.2: A Climate Model Optimized for the Middle Atmosphere—Model Structure, Climatology, Variability, and Climate Sensitivity. *Journal of Geophysical Research: Atmospheres*, *125*(10).

Rind, D., Suozzo, R., Balachandran, N. K., Lacis, A., & Russell, G. (1988). The

GISS global climate-middle atmosphere model. Part I: model structure and climatology. *Journal of the Atmospheric Sciences*, *45*(3), 329–370.

Robock, A. (2000). Volcanic Eruptions and Climate. *Reviews of Geophysics*, *38*(2), 191–219.

Robock, A., & Mao, J. (1995). The volcanic signal in surface temperature observations. *Journal of Climate*, *8*, 1086–1103.

Stenchikov, G., Robock, A., Ramaswamy, V., Schwarzkopf, M. D., Hamilton, K., & Ramachandran, S. (2002). Arctic Oscillation response to the 1991 Mount Pinatubo eruption: Effects of volcanic aerosols and ozone depletion. *Journal of Geophysical Research Atmospheres*, *107*(24), 1–16.

Thomason, L. W., Ernest, N., Millán, L., Rieger, L., Bourassa, A., Vernier, J. P., ... Peter, T. (2018). A global space-based stratospheric aerosol climatology: 1979–2016. *Earth System Science Data*, *10*(1), 469–492.

Tie, X., & Brasseur, G. (1995). The response of stratospheric ozone to volcanic eruptions: Sensitivity to atmospheric chlorine loading. *Geophys. Res. Lett.*, *22*(22), 3035–3038.

Tweedy, O. V., Kramarova, N. A., Strahan, S. E., Newman, P. A., Coy, L., Randel, W. J., ... Frith, S. M. (2017). Response of trace gases to the disrupted 2015–2016 quasi-biennial oscillation. *Atmospheric Chemistry and Physics*, *17*(11), 6813–6823.